IEEE Access
Multidisciplinary | Rapid Review | Open Access Journal

Received April 11, 2019, accepted May 3, 2019, date of publication May 8, 2019, date of current version June 3, 2019.

Digital Object Identifier 10.1109/ACCESS.2019.2915506

Robust Interacting Multiple Model With Modeling Uncertainties for Maneuvering Target Tracking

WONKEUN YOUN[1,2], (Member, IEEE), AND HYUN MYUNG[2], (Senior Member, IEEE)
[1]UAV System Division, Aeronautics Research and Development Head Office, Korea Aerospace Research Institute, Daejeon 34133, South Korea
[2]Urban Robotics Laboratory (URL), Korea Advanced Institute of Science and Technology (KAIST), Daejeon 34141, South Korea

Corresponding author: Hyun Myung (hmyung@kaist.ac.kr)

This work was supported in part by the Unmanned Vehicles Advanced Core Technology Research and Development Program (Development of the Open Architecture-based, Integrated Computer for Flight Control and Multi-mission of small drones) through the National Research Foundation of Korea (NRF), in part by the Unmanned Vehicle Advanced Research Center (UVARC) through the Ministry of Science and ICT, South Korea under Grant 2016M1B3A1A03937484, and in part by the Korea Agency for Infrastructure Technology Advancement (KAIA) through the Ministry of Land, Infrastructure, and Transport under Grant 18USTR-B127901-02.

ABSTRACT This paper proposes an improved robust interacting multiple model (RIMM) algorithms with modeling uncertainties for maneuvering target tracking with changing dynamics. To mitigate the effects of the modeling uncertainty, a compensation step is introduced to adjust the degree of dependence of the filtering on the system or the measurement model based on the orthogonality principle between the state estimation error and innovation sequence of the subfilter model in the RIMM algorithm. By relying on the compensation parameter, the proposed algorithm fully utilizes the useful information in the innovation sequence and reduces the impact of system model error. The numerical simulation and car-mounted experiments using time difference of arrival (TDOA) measurements of the maneuvering target tracking with changing dynamics are conducted to verify the effectiveness of the proposed RIMM algorithm. Compared with the conventional approaches, the proposed RIMM algorithm results in a remarkable improvement in the state estimation accuracy and small bias while improving the consistency of the filter.

INDEX TERMS Robust interacting multiple model, maneuvering target tracking, modeling uncertainties, orthogonality principle, unscented Kalman filter, extended Kalman filter.

I. INTRODUCTION

Maneuvering target tracking with changing dynamics has been widely investigated in various applications such as aircraft traffic control (ATC) [1], multiple target tracking/recognition [2], road vehicle navigation [3], and spacecraft detection/characterization [4]. Because of the characterization complexity and diversity of maneuvering target trajectories, a standard Kalman filter designed using a single dynamic model with constant parameters - process and measurement noise - does not achieve satisfactory performance when the mode of the maneuvering target varies unexpectedly [5].

To resolve this mode-changing problem, a variety of methods have been investigated, such as the interacting multiple model (IMM) algorithm [6], the α-β filter [7], and the track-before-detect (TBD) algorithm [8]. Among these approaches, the IMM algorithm has attracted substantial attention in the past few decades [6]. The IMM algorithm runs a number of subfilter models in parallel to obtain a better state estimate of a system with changing dynamics [6]. In addition, the model-matched subfilters in the IMM filter interact with each other, leading to improved estimation results [9].

The linear/nonlinear dynamic systems in the IMM subfilter consist of the system and measurement models [10]. The system model defines the mathematical model of the physical phenomena of the system state variables, whereas the measurement model represents the information measured by sensors. Because the system model is only an approximation based on the physical interpretation of the true system, modeling errors are inevitable in practical problems. An incorrect model may affect the estimation performance of the filter and may even cause the filter to diverge [11].

II. RELATED WORKS

To deal with model uncertainty, various promising approaches, such as the innovation-based adaptive Kalman

The associate editor coordinating the review of this manuscript and approving it for publication was Rui-Jun Yan.

2169-3536 © 2019 IEEE. Translations and content mining are permitted for academic research only.
Personal use is also permitted, but republication/redistribution requires IEEE permission.
See http://www.ieee.org/publications_standards/publications/rights/index.html for more information.

filter [12], noise covariance matching filter [13], fading memory filter [14], and Sage-Husa adaptive Kalman filter [15], have been proposed. However, both the innovation-based adaptive Kalman filter and noise covariance matching filters have the drawback of high computational complexity. The traditional Sage-Husa Kalman filter cannot guarantee the convergence of the solution [15]. In addition, the abovementioned algorithms have only been implemented in single-model systems and have not been demonstrated to be suitable solutions for multiple-model changing systems with modeling uncertainties.

To address the modeling uncertainty, a Student's t distribution-based robust filtering algorithm has recently been proposed [16]. Student's t distribution has heavy tails when the degree of freedom (DOF) parameter is less than infinity, which makes it more suitable to model heavy-tailed process noise. The robust Student's t-based third-degree cubature Kalman filter has been proposed to suppress the process and measurement noise [17]. A Student's t-based Kalman filter has also been investigated for linear systems with heavy-tailed process and measurement noises for a maneuvering target tracking simulation [18]. In addition, a robust fixed-interval smoother based on Student's t distribution for heavy-tailed process and measurement noises has been investigated using a variational Bayesian approach [19]. However, the aforementioned approaches require several complicated tuning parameters and a fixed calculation iteration to infer the latent variables, limiting the capability for real-time computation.

In addition, the design of a reasonable subfilter model set in the IMM algorithm is one of the most challenging tasks in practical applications [20]. Because the system always operates in a surrounding environment with uncertainty, it is not practical to include all possible system models to address the modeling uncertainty [21]. Moreover, a large number of subfilter models does not always guarantee an improvement of the estimation performance. In fact, it has been reported that the estimation performance of the IMM algorithm is degraded significantly if too many models are implemented in the subfilter [21].

To the best of our knowledge, few studies have employed robust algorithms for single-model target tracking problems with model mismatch, and very few studies have investigated the feasibility of robust algorithms for target tracking problems with changing dynamics subject to uncertain modeling parameters. In this paper, we propose a novel robust IMM algorithm for multiple-model systems with modeling uncertainties. In contrast to the aforementioned methods, an uncertainty compensation step is introduced to ensure that the errors of the state estimation in the dominating subfilter model are orthogonal to the innovation sequence as much as possible, leading to a higher estimation accuracy and consistency of the filter. The performance of the proposed RIMM algorithm is demonstrated by comparison with the conventional IMM approach.

III. THE ROBUST INTERACTING MULTIPLE-MODEL FILTER

Consider the following discrete stochastic hybrid system of the j-th model belonging to the subfilter model set:

$$x^j(k+1) = f^j\left(x^j(k), u_k\right) + \Gamma^j w^j(k) \tag{1}$$

$$z(k) = h\left(x^j(k)\right) + \upsilon(k) \tag{2}$$

where k is the time index, $x^j(k)$ the state vector, $z^j(k)$ the measurement vector, u_k the input variable, $w^j(k)$ the process noise, $\upsilon(k)$ the measurement noise, $E\left[w^j(k)w^j(l)^T\right] = Q(k)\delta_{kl}$, $E\left[\upsilon^j(k)\upsilon^j(l)^T\right] = R(k)\delta_{kl}$, $E\left[w^j(k)\upsilon^j(l)^T\right] = 0$, $f^j(\cdot)$ the system model function, Γ^j the noise excitation matrix, and $h(\cdot)$ the measurement function. In this paper, $f^1(\cdot)$ nd $f^2(\cdot)$ denote the uniform motion model and the coordinated turn model, respectively. The details of the subfilter model are provided in Section V.

The IMM algorithm uses a recursive algorithm composed of the following four sequential processes: (1) interaction/mixing process, (2) filtering, (3) model probability update, and (4) estimate and covariance combination [5]. All possible system behaviors are denoted by a set of models $M = \{1, 2, \ldots, N_r\}$, where N_r is the total number of models. The transition probability from the i-th model, M_i, to the j-th model, M_j, is represented as

$$p_{ij} = P\left\{M_j(k) | M_i(k-1)\right\}$$

where $i, j \in \{1, 2, \cdots, N_r\}$.

A. INTERACTION/MIXING PROCESS

The mixing probability that model M_i was in effect at time $k-1$ given that model M_j is in effect at time k conditioned on $Z^{k-1} \equiv \{z_i\}_{i=1}^{k-1}$ can be obtained using the transition probability, p_{ij}, as follows [22]:

$$\mu^{ij}(k-1|k-1) = \frac{1}{\bar{c}_j} p_{ij}\mu^i(k-1) \tag{3}$$

where the normalizing constant is

$$\bar{c}_j = \sum_{i=1}^{N_r} p_{ij}\mu^i(k-1).$$

Starting with the previous estimate $\hat{x}(k-1|k-1)$, the mixed state $\hat{x}^{0j}(k-1|k-1)$ and mixed covariance $P^{0j}(k-1|k-1)$ of each subfilter model can be obtained using the mixing probabilities as follows:

$$\hat{x}^{0j}(k-1|k-1) = \sum_{i=1}^{N_r} \mu^{ij}(k-1|k-1)\hat{x}^i(k-1|k-1)$$

$$P^{0j}(k-1|k-1) = \sum_{i=1}^{N_r} \mu^{ij}(k-1|k-1) \cdot \begin{pmatrix} P^i(k-1|k-1) + [\hat{x}^i(k-1|k-1) - \\ \hat{x}^{0j}(k-1|k-1)] \cdot [\hat{x}^i(k-1|k-1) - \\ \hat{x}^{0j}(k-1|k-1)]^T \end{pmatrix}. \tag{4}$$

B. FILTERING PROCESS

The individual subfiltering process of the IMM filter is the same as that of the standard Bayesian filter. Among the various filtering approaches, the extended Kalman filter (EKF) is the most widely utilized approach to handle state estimation for nonlinear systems. The EKF runs on the basis of the first-order Taylor expansion to approximate the means and covariances of the true nonlinear system. Thus, the EKF might suffer from several critical issues such as large initial state estimation errors, the need to calculate the Jacobian and Hessian matrices and poor robustness against incorrect system modeling [23].

The unscented Kalman filter (UKF) is an extension of the classical EKF to nonlinear estimation [24]. The time propagation of the state and state error covariance of the UKF is performed based on an unscented transformation that realistically estimates the probability density of the state distribution, avoiding the calculation of the Jacobian and Hessian matrices and thus making the UKF algorithm easier to implement. In particular, the UKF can achieve greatly improved estimation performance and robustness to large initial state estimation errors compared with the EKF filter for nonlinear systems [25]. Thus, either the EKF and UKF filter can be used as the individual subfilter of the IMM filter in this paper. It should be noted that the mixed state $\hat{x}^{0j}(k-1|k-1)$ and mixed covariance $P^{0j}(k-1|k-1)$ are utilized as the inputs in the following EKF/UKF subfiltering.

1) EXTENDED KALMAN FILTER

To obtain the prior mean state $\hat{x}^j(k|k-1)$ and the covariance $P^j(k|k-1)$ of the j-th subfilter, the standard EKF is adapted as follows [26]:

$$\begin{aligned}\hat{x}^j(k|k-1) &= f^j\left(\hat{x}^{0j}(k-1|k-1), u_{k-1}\right)\\ P^j(k|k-1) &= F^j(k-1)P^{0j}(k-1|k-1)F^j(k-1)^T\\ &\quad + \Gamma^j(k-1)Q^j(k-1)\Gamma^j(k-1)^T\end{aligned}$$

where

$$F^j(k-1) = \left.\frac{\partial f^j}{\partial x}\right|_{x=\hat{x}^{0j}(k-1|k-1).}$$

The innovation covariance matrix $S^j(k)$ can be described as

$$S^j(k) = H^j(k)P^j(k|k-1)H^j(k)^T + R(k)$$

where

$$\begin{aligned}H^j(k) &= \left.\frac{\partial h^j}{\partial x}\right|_{x=\hat{x}^j(k|k-1)}\\ K^j(k) &= P^j(k|k-1)H^j(k)^T S^j(k)^{-1}\\ \nu^j(k) &= z(k) - h^j\left(\hat{x}^j(k|k-1)\right).\end{aligned}$$

The posterior state and the corresponding error covariance are updated as follows:

$$\begin{aligned}P^j(k|k) &= P^j(k|k-1) - K^j(k)S^j(k)K^j(k)^T\\ \hat{x}^j(k|k) &= \hat{x}^j(k|k-1) + K^j(k)\nu^j(k).\end{aligned} \tag{5}$$

2) UNSCENTED KALMAN FILTER

Unscented transformation (UT) is the core statistical technique of the UKF [24] and is used to address the nonlinearity in a nonlinear system model $y = f(x)$, where x and y are $L \times 1$ vectors, f is an $L \times 1$ vector-valued function, and L is the length of the state vector. Using three scaling parameters (i.e., α, β, and κ), an additional scaling parameter, λ, and weight vectors for the i-th sigma point, the η_i^m (mean) and η_i^c (covariance) are defined, and the standard nonaugmented UKF [27] is adopted here.

$$\begin{cases}\lambda = \alpha^2(L+\kappa) - L\\ \eta_0^m = \lambda/(L+\lambda)\\ \eta_0^c = \lambda/(L+\lambda) + 1 - \alpha^2 + \beta\\ \eta_i^m = \eta_i^c = 1/[2(L+\lambda)], i = 1, \cdots, 2L.\end{cases}$$

The parameter λ, the prior mean $\hat{x}^j(k-1|k-1)$, and the covariance $P^j(k-1|k-1)$ are then used to generate $2L+1$ sigma points as follows:

$$\begin{aligned}\chi_{i,k-1}^j &= \hat{x}^{0j}(k-1|k-1)\\ &\quad + \begin{cases}0 & \text{for } i = 0\\ \sqrt{(L+\lambda)P^{0j}(k-1|k-1)} & \\ \quad \text{for } i = 1, \cdots, L & \\ -\sqrt{(L+\lambda)P^{0j}(k-1|k-1)} & \\ \quad \text{for } i = L, \cdots, 2L.\end{cases}\end{aligned} \tag{6}$$

where $\sqrt{P}$ can be calculated through the Cholesky decomposition of the covariance matrix.

The sigma point χ_i is processed through the nonlinear system model to generate a transformed sample, and the mean and covariance of the predicted state can be calculated as

$$\begin{aligned}\hat{\chi}_{i,k|k-1}^j &= f(\chi_{i,k-1}^j, u_k), \quad i = 0, 1, \cdots, 2L\\ \hat{x}^j(k|k-1) &= \sum_{i=0}^{2L} \eta_i^m \hat{\chi}_{i,k|k-1}^j\\ P^j(k|k-1) &= \sum_{i=0}^{2L} \eta_i^c \left(\hat{\chi}_{i,k|k-1}^j - \hat{x}^j(k|k-1)\right)\\ &\quad \cdot \left(\hat{\chi}_{i,k|k-1}^j - \hat{x}^j(k|k-1)\right)^T + Q(k-1)\end{aligned}$$

A set of new sigma points $\chi_{i,k|k-1}^j$ is re-selected based on the mean $\hat{x}^j(k|k-1)$ and the corresponding covariance $P^j(k|k-1)$ similar to (6), and the transformed sigma points for measurement are:

$$\hat{\psi}_{i,k|k-1}^j = h\left(\chi_{i,k|k-1}^j, u_k\right), \quad i = 0, 1, \cdots, 2L$$

The predicted measurement and its corresponding covariance matrix are described as

$$\hat{z}(k|k-1) = \sum_{i=0}^{2L} \eta_i^m \hat{\psi}_{i,k|k-1}$$
$$P_{zz}^j(k) = \sum_{i=0}^{2L} \eta_i^c \left(\hat{\psi}_{i,k|k-1}^j - \hat{z}^j(k|k-1)\right) \cdot \left(\hat{\psi}_{i,k|k-1}^j - \hat{z}^j(k|k-1)\right)^T + R(k-1).$$

The cross-covariance between the predicted state and measurement can be calculated as

$$P_{xz}^j(k) = \sum_{i=0}^{2L} \eta_i^c \left(\hat{\chi}_{i,k|k-1}^j - \hat{x}^j(k|k-1)\right) \cdot \left(\hat{\psi}_{i,k|k-1}^j - \hat{z}^j(k|k-1)\right)^T$$
$$K^j(k) = P_{xz}^j(k) P_{zz}^j(k)^{-1}$$
$$\nu^j(k) = z^j(k) - \hat{z}^j(k|k-1)$$

The state estimate $\hat{x}(k|k)$ and corresponding error state covariance matrix $P(k|k)$ are updated as follows:

$$P^j(k|k) = P^j(k|k-1) - K^j(k) P_{zz}^j(k) (K(k)^j)^T$$
$$\hat{x}^j(k|k) = \hat{x}^j(k|k-1) + K^j(k)\nu^j(k). \quad (7)$$

C. MODEL PROBABILITY UPDATE PROCESS

The model probability $\mu^i(k)$ is updated according to the model likelihood and model transition probability by

$$\mu^i(k) = \frac{1}{c}\Lambda_i(k)\bar{c}_i, \quad i = 1, \cdots, N_r$$

where

$$c = \sum_{i=1}^{N_r} \Lambda_i(k)\bar{c}_i$$

and $\Lambda_i(k)$ is a likelihood function given by

$$\Lambda_i(k) = \frac{1}{\sqrt{|2\pi S^i(k)|}} \exp\left(-\frac{1}{2}\nu^i(k)^T S^i(k)^{-1}\nu^i(k)\right).$$

D. COMBINATION PROCESS

The state estimates and covariance of the subfilter model are combined into the overall state and covariance as follows:

$$\hat{x}(k|k) = \sum_{i=1}^{N_r} \mu^i(k)\,\hat{x}^i(k|k)$$
$$P(k|k) = \sum_{i=1}^{N_r} \mu^i(k) \left(P^i(k|k) + (\hat{x}^i(k|k) - \hat{x}(k|k)) \cdot (\hat{x}^i(k|k) - \hat{x}(k|k))^T\right).$$

The detailed derivation of the IMM algorithm is given in [22].

IV. COMPENSATION ALGORITHM FOR MODELING UNCERTAINTY IN THE IMM FILTER

The proposed compensation algorithm for modeling uncertainty in the IMM filter is motivated by the basic idea of the strong tracking filter (STF) [28]. However, the original STF approach is not directly applicable to the multimodel-based estimation problem since the STF does not consider the effect of the interaction between models in a multimodel problem. Thus, the proposed compensation algorithm is modified to address the subfilter model of the IMM filter to handle the multimodel-based estimation problem with modeling uncertainty.

A. BRIEF REVIEW OF THE ORTHOGONAL PRINCIPLE IN THE IMM FILTER

Let $\varepsilon^j(k) = x(k) - \hat{x}^j(k|k)$ be the state estimation error in the j-th subfilter at time k, and assume that $E\left[\varepsilon^j(k)\,\nu^j(k)^T\right] = 0$. In the standard Kalman filter where the mode sequence for the model is available, it is straightforward to prove that the estimation error $\varepsilon^j(k)$ is orthogonal to its innovation $\nu^j(k)$. Reference [29], [30] demonstrated that the estimation error $\varepsilon^j(k)$ is also orthogonal to its innovation $\nu^j(k)$ in the j-th subfilter model of the IMM filter when the system model is correct, which is used to derive the model uncertainty compensation algorithm in the following subsection.

For the clarity and completeness of the remainder of this subsection, the orthogonality principle of the j-th subfilter model of the IMM filter derived in reference [29], [30] is briefly reviewed. In this subsection, instead of a nonlinear system and measurement equation, we use a linear system and measurement equation for simplicity (i.e., $x^j(k+1) = A^j x^j(k) + \Gamma^j w^j(k)$, $z^j(k) = H^j x^j(k) + \upsilon(k)^j$).

The model-matched subfilter determines primarily the estimation performance of the IMM filter, as the mode probabilities of the unmatched subfilters are relatively small. Therefore, when calculating the inner product of the innovation sequence under the true subfilter models $\tilde{i}$ and $\tilde{j}$ at time instants $k-1$ and k, respectively, defined as $I^{<\tilde{j},\,\tilde{i}>}(k|k-1)$, the innovation sequence of the unmatched subfilters can be neglected, thus yielding the following [30]:

$$I^{<\tilde{j},\,\tilde{i}>}(k|k-1) = E\left[\nu^{\tilde{j}}(k)\,\nu^{\tilde{i}}(k-1)^T\right] \quad (8)$$

where $\nu^{\tilde{j}}(k) = z(k) - H^{\tilde{j}}(k)\hat{x}^{\tilde{j}}(k|k-1)$ is the innovation sequence in the $\tilde{j}$-th subfilter model. Substituting $x(k)$ and $z(k)$ into the system and measurement equations yields

$$\begin{aligned} &I^{<\tilde{j},\,\tilde{i}>}(k|k-1) \\ &= E\left[\left(z(k) - H^{\tilde{j}}\hat{x}^{\tilde{j}}(k|k-1)\right)\nu^{\tilde{i}}(k-1)^T\right] \\ &= E\left[H^{\tilde{j}}\left(x(k) - \hat{x}^{\tilde{j}}(k|k-1)\right)\nu^{\tilde{i}}(k-1)^T\right] \\ &= H^{\tilde{j}}A^{\tilde{j}}\,E\left[\left(x(k-1) - \hat{x}^{0\tilde{j}}(k-1|k-1)\right)\nu^{\tilde{i}}(k-1)^T\right] \end{aligned} \quad (9)$$

where $\hat{x}^{0\tilde{j}}(k-1|k-1)$ is the mixed input to the j-th subfilter. In the standard Kalman filter, it is straightforward to verify

that (9) equals zero (i.e., $I^{<\tilde{j},\ \tilde{i}>}(k|k-1)=0$). However, the input $\hat{x}^{0\tilde{j}}(k-1|k-1)$ to the subfilter in the IMM filter, in contrast to $\hat{x}(k-1|k-1)$, is computed by mixing all previous estimates according to the corresponding mode probability $\mu^{\tilde{i}\tilde{j}}(k-1|k)$. In this sense, (9) is no longer equal to zero [29]. According to (3), the mode probability $\mu^{\tilde{i}\tilde{j}}(k-1|k)$ satisfies the following property:

$$\sum_{i=1}^{N_r}\mu^{\tilde{i}\tilde{j}}(k-1|k)\ =\ 1.$$

With this property, $I^{<\tilde{j},\ \tilde{i}>}(k|k-1)$ specified by (9) can be equivalently rewritten as

$$I^{<\tilde{j},\ \tilde{i}>}(k|k-1) = H^{\tilde{j}}A^{\tilde{j}}\sum_{i=1}^{N_r}\mu^{\tilde{i}\tilde{j}}(k-1|k)E\left[\varepsilon^{i}(k-1)\,v^{\tilde{i}}(k-1)^T\right]. \tag{10}$$

By extracting the terms with respect to the true mode i, (10) becomes

$$\begin{aligned}I^{<\tilde{j},\ \tilde{i}>}(k|k-1) &= H^{\tilde{j}}A^{\tilde{j}}\,\mu^{\tilde{i}\tilde{j}}(k-1|k)\ E\left[\varepsilon^{\tilde{i}}(k-1)\,v^{\tilde{i}}(k-1)^T\right]\\ &\quad + H^{\tilde{j}}A^{\tilde{j}}\sum_{i=1,i\neq\tilde{i}}^{N_r}\mu^{\tilde{i}\tilde{j}}(k-1|k)E\left[\varepsilon^{i}(k-1)v^{\tilde{i}}(k-1)^T\right].\end{aligned} \tag{11}$$

In addition, the term $\varepsilon^{\tilde{i}}(k-1)$ in (11) can be decomposed as

$$\varepsilon^{\tilde{i}}(k-1)=x(k-1)-\hat{x}^{\tilde{i}}(k-1|k-2)-K^{\tilde{i}}(k-1)v^{\tilde{i}}(k-1)$$

where $\hat{x}^{\tilde{i}}(k-1|k-2)$ is the predicted estimate at time $k-1$ and $K^{\tilde{i}}(k-1)$ is the corresponding Kalman gain. Following the definition of the innovation sequence, we obtain

$$v^{\tilde{i}}(k-1)\ =H^{\tilde{i}}\left[x(k-1)-\hat{x}^{\tilde{i}}(k-1|k-2)\right]+v\,(k-1).$$

We introduce an intermediate variable, $\Xi^{\tilde{i}}(k-1)$, as

$$\begin{aligned}\Xi^{i}(k-1) &= E\left[\varepsilon^{\tilde{i}}(k-1)v^{\tilde{i}}(k-1)^T\right]\\ &= E\left[\begin{array}{c}\left(x(k-1)-\hat{x}^{\tilde{i}}(k-1|k-2)\right)\\ \cdot\left(x(k-1)-\hat{x}^{\tilde{i}}(k-1|k-2)\right)^T\end{array}\right]H^{\tilde{i}}(k-1)^T\\ &\quad - K^{\tilde{i}}(k-1)E\left[v^{\tilde{i}}(k-1)v^{\tilde{i}}(k-1)^T\right]\\ &= P(k-1|k-2)H^{\tilde{i}}(k-1)^T - K^{\tilde{i}}(k-1)S^{\tilde{i}}(k-1).\end{aligned}$$

The Kalman gain can be computed by

$$K^{\tilde{i}}(k-1)=P^{\tilde{i}}(k-1|k-2)H^{\tilde{i}}(k-1)^T S^{\tilde{i}}(k-1)^{-1}. \tag{12}$$

Thus, we can obtain the following result [30]:

$$\Xi^{\tilde{i}}(k-1)=0. \tag{13}$$

Equation (13) implies that the estimation error $\varepsilon^{\tilde{i}}(k)$ with respect to the $\tilde{i}$-th model is orthogonal to the corresponding innovation $v^{\tilde{i}}(k)$ if the model used in the filter perfectly matches the true model [30]. This important property provides the basis for deriving the modeling uncertainty compensation algorithm of the IMM filter in the following subsection.

B. MODELING UNCERTAINTY COMPENSATION ALGORITHM

According to the orthogonality principle in (13), the estimation error is orthogonal to the innovation sequence when the theoretical subfilter model in the IMM filter exactly matches the actual true model [31]. However, with uncertain model parameters, (13) is no longer a valid property because (8) cannot be transformed into (9). Thus, a time-variant compensation parameter for modeling the uncertainty λ is introduced as in [32], which modifies the mixed variance $P^{0j}(k-1|k-1)$ specified by (4) before filtering as

$$\begin{aligned}\bar{P}^{0j}(k|k-1)=&\lambda^{j}(k-1)F^{j}(k-1)P^{0j}(k-1|k-1)F^{j}(k-1)^T\\ &+\Gamma^{j}(k-1)Q^{j}(k-1)\Gamma^{j}(k-1)^T\end{aligned} \tag{14}$$

where $\bar{P}$ denotes the modified variance by the uncertainty compensation operation.

To satisfy the orthogonal principle, λ^{j} must be determined to satisfy (13) under the dominating subfilter of the IMM filter. This is similar to approaches like [28] and [33] that add artificial process noise into the state prediction error covariance of the Kalman filter to improve the estimation accuracy when there is a modeling mismatch, thus making the innovation sequence orthogonal to the estimation error. The filter can achieve a better balance between dependence on the system and dependence on the measurement by adjusting the Kalman gain $K^{j}(k)$ adaptively to yield a higher robustness to system model uncertainty. According to (5) and (7), $K^{j}(k)$ represents the Kalman gain matrix of the j-th dominating model, and $v^{j}(k)$ represents the innovation sequence of the j-th model. As reviewed in the previous subsection, to ensure that the innovation sequence $v^{j}(k)$ is orthogonal to the state estimation error $\varepsilon^{j}(k)$, (13) should be satisfied as follows:

$$\Xi^{j}(k)=E\left[\varepsilon^{j}(k)\,v^{j}(k)^T\right]=0. \tag{15}$$

Substituting the prior state estimation error $\bar{\varepsilon}^{j}(k)\ =\ x(k)-\hat{x}^{j}(k|k-1)$ into (15),

$$\begin{aligned}E\left[\varepsilon^{j}(k)v^{j}(k)^T\right] &= E\left[(\bar{\varepsilon}^{j}(k)-K^{j}(k)v^{j}(k))v^{j}(k)^T\right]\\ &= E\left[\bar{\varepsilon}^{j}(k)v^{j}(k)^T\right]-K^{j}(k)E\left[v^{j}(k)\,v^{j}(k)^T\right].\end{aligned}$$

Using the measurement equation (2), $v^{j}(k)$ can be written as

$$v^{j}(k)=H^{j}(k)(x(k)-\hat{x}^{j}(k|k-1))+\upsilon(k)$$

$$= H^j(k)\bar{\varepsilon}^j(k) + \upsilon(k),$$

which further results in

$$E\left[\varepsilon^j(k)\nu^j(k)^T\right] = E\left[\bar{\varepsilon}^j(k)(H^j(k)\bar{\varepsilon}^j(k) + \nu(k))^T\right] - K^j(k)E\left[\nu^j(k)\nu^j(k)^T\right].$$

Let $S^j(k) = E\left[\nu^j(k)\,\nu^j(k)^T\right]$. Because $\bar{\varepsilon}^j(k)$ and $\nu(k)$ are independent for $k \geq 0$,

$$\begin{aligned} &E\left[\varepsilon^j(k)\nu^j(k)^T\right] \\ &= E\left[\bar{\varepsilon}^j(k)(H^j(k)\bar{\varepsilon}^j(k))^T\right] - K^j(k)S^j(k) \\ &= P^{0j}(k|k-1)H^j(k)^T - K^j(k)S^j(k), \end{aligned}$$

which together with (12) yields that (15) can be rewritten as

$$\begin{aligned} &E\left[\varepsilon^j(k)\nu^j(k)^T\right] \\ &= P^{0j}(k|k-1)H^j(k)^T \\ &\cdot\left[I - (H^j(k)P^{0j}(k|k-1)H^j(k)^T + R(k))^{-1}S^j(k)\right] = 0. \end{aligned} \tag{16}$$

A sufficient condition for (16) to be satisfied can be expressed as follows:

$$H^j(k)P^{0j}(k|k-1)\,H^j(k)^T = S^j(k) - R(k). \tag{17}$$

Substituting (14) into (17), the above equation can be expressed as

$$\begin{aligned} &\lambda^j(k)H^j(k)F^j(k-1)P^{0j}(k-1|k-1)F^j(k-1)^T H^j(k)^T \\ &= S^j(k) - H^j(k)\Gamma^j(k-1)Q^j(k-1)\Gamma^j(k-1)^T H^j(k)^T \\ &\quad - R(k). \end{aligned} \tag{18}$$

$\lambda^j(k) \geq 0$ exists only when the term on the right-hand side of (18) is a positive semidefinite matrix. To improve the smoothness of the state estimation $\hat{x}(k)$, a softening factor $\alpha \geq 1$ is introduced into (18) [29], [34], and rearranging the term yields

$$\lambda^j(k)\,\Theta^j(k) = U^j(k) \tag{19}$$

where

$$\begin{aligned} \Theta^j(k) &= H^j(k)F^j(k-1)P^{0j}(k-1|k-1)F^j(k-1)^T \\ &\quad \cdot H^j(k)^T, \\ U^j(k) &= S^j(k) - H^j(k)\Gamma^j(k-1)Q^j(k-1)\Gamma^j(k-1)^T \\ &\quad \cdot H^j(k)^T - \alpha R(k). \end{aligned} \tag{20}$$

Taking the trace operation on both sides of (19), the equivalent formulation is [29]

$$\lambda^j(k) = \frac{tr\left(U^j(k)\right)}{tr\left(\Theta^j(k)\right)}. \tag{21}$$

According to [28], $S^j(k)$ can be defined as

$$S^j(k) = \begin{cases} \nu^j(k)\nu^j(k)^T & \text{if } k = 1 \\ \dfrac{\rho S^{0j}(k-1) + \nu^j(k)\nu^j(k)^T}{1+\rho} & \text{if } k \geq 2 \end{cases}$$

where $0 < \rho < 1$ is a softening factor designed to give less weight to older variances [34], and it is selected by experience as, e.g., 0.95. $S^{0j}(k-1)$ is specified by

$$S^{0j}(k-1) = \sum_{i=1}^{N_r} \mu^{ij}(k-1|k-1)\,S^j(k-1).$$

From (14), we can see the effect of $\lambda \geq 1$ in increasing the reliance of the subfilter j-th model on the measurement relative to the system model. Specifically, by multiplying the prior covariance by the model compensation parameter λ in the j-th subfilter of the IMM filter, the information of the system model is weighted less, and hence, the information of the measurement model is weighted more. More specifically, if there is no significant system model error, λ remains one, and it does not influence the estimation performance. On the other hand, $\lambda \geq 1$ indicates that the model utilized in the subfilter does not exactly coincide with the model of the true system.

However, the true system can be reflected primarily under the j-th dominating subfilter model of the IMM filter [30]. Therefore, compensating $P^{0j}(k-1|k-1)$ from (14) with λ may considerably reduce the distinctive separation between the matched and unmatched subfilter models of the IMM filter [29]. In addition, the compensation parameter under the matched subfilter models in the IMM filter should be smaller than that of the other subfilter models. Thus, to overcome this drawback [29], [30], the following additional minimization step is introduced:

$$\lambda(k) = \min_i \lambda^i(k). \tag{22}$$

Note that λ may be less than 1 in (22). To avoid such a circumstance, λ can be further taken as

$$\bar{\lambda}(k) = \max(1,\ \lambda(k)).$$

Fig. 1 provides a basic operational diagram of the proposed RIMM-based estimation. The proposed RIMM-based algorithm has obvious significance; when there are noticeable discrepancies between the true system model and the subfilter model used in the IMM filter, the innovation sequence is constrained to be orthogonal to the estimation error by adaptively tuning the Kalman gain. This implies that all important information in the innovation sequence is utilized so that the proposed algorithm has strong robustness to modeling uncertainties.

To calculate the time-variant compensation parameter of the EKF, we need to calculate the linearization of the nonlinear system and measurement matrix. However, the calculation of the Jacobian or Hessian matrix is not required in

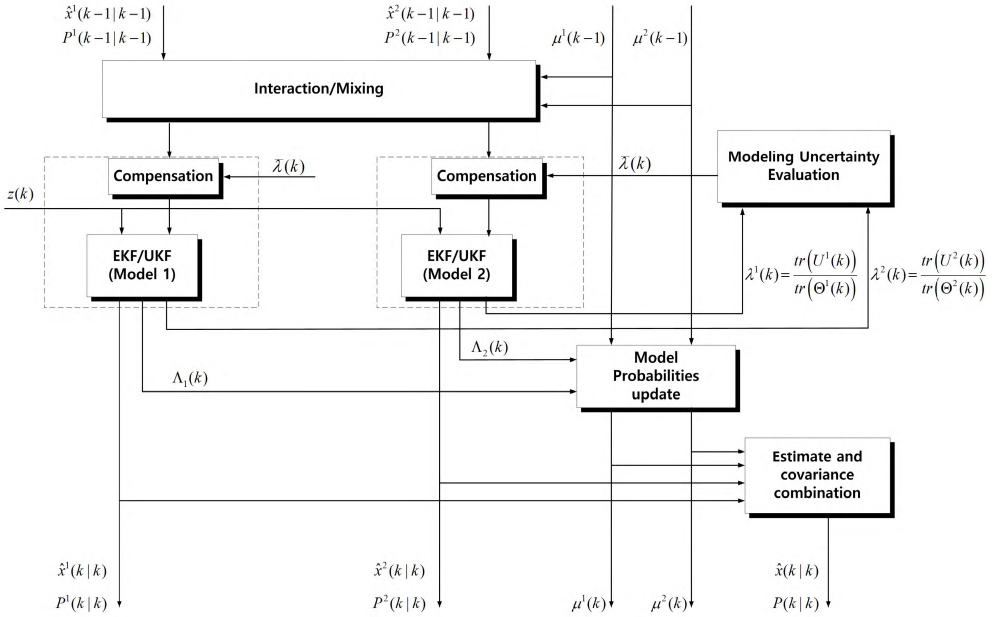

FIGURE 1. Basic operational diagram of the proposed robust IMM algorithm with modeling uncertainty.

the UKF. The equivalent expression of the time-variant compensation parameter for (20) can be expressed as follows [35]:

$$\begin{aligned} P^{xz}(k) &= E\left[(x(k)-\hat{x}(k|k-1))(z(k)-\hat{z}(k|k-1))^T\right] \\ &= E\left[(\bar{\varepsilon}(k))(H(k)\bar{\varepsilon}(k)+v(k))^T\right] \\ &= E\left[\bar{\varepsilon}(k)\bar{\varepsilon}(k)^T\right]H(k)^T + E\left[\bar{\varepsilon}(k)v(k)^T\right] \\ &= P(k|k-1)H(k)^T. \end{aligned} \tag{23}$$

where $P(k|k-1)$ is the state error covariance matrix before introducing the compensation parameter, $P^j_{zz}(k)$ is the measurement covariance matrix, and $P^j_{xz}(k)$ is the cross-covariance matrix. Substituting $H(k) = P^j_{xz}(k)^T (P^j(k|k-1))^{-1}$ from (23) into (20), we can obtain the following equivalent equation for the UKF.

$$\begin{aligned} U^j(k) &= S^j(k) - P^j_{xz}(k)^T (P^j(k|k-1))^{-1}\Gamma^j(k-1) \\ &\quad \cdot Q^j(k-1)\Gamma^j(k-1)^T (P^j(k|k-1))^{-1} P^j_{xz}(k) - \alpha R(k) \\ \Theta^j(k) &= P^j_{zz}(k) - S^j(k) + U^j(k) + (\alpha-1)R(k). \end{aligned} \tag{24}$$

The time-variant compensation parameter of the UKF can be obtained by (24). It can be observed that the calculation of the time-variant compensation parameter in the above expression does not require a Jacobian or Hessian matrix to be computed. The cumulative numerical errors from the iterative modification of the mixed variance $P^{0j}(k-1|k-1)$ specified by (4) can result in a loss of symmetry or loss of positive definiteness [36]. Thus, the following equation is utilized to guarantee positive-definite and symmetric covariance matrices after the operation of (4) [37]:

$$P \longleftarrow \frac{1}{2}(P + P^T).$$

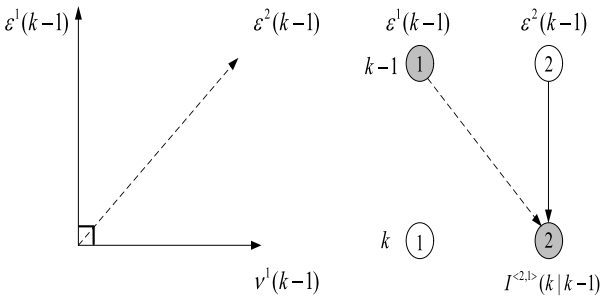

FIGURE 2. Illustration of the orthogonal principle and $I^{<\tilde{j},\,\tilde{i}>}(k|k-1)$ with two nodes [30].

Example 1: Suppose that a different model 1 and model 2 are running simultaneously in the proposed IMM algorithm at times $k-1$ and k, as shown in Fig. 2, where the true node is highlighted in gray. It is shown that the estimation error $\varepsilon^1(k-1)$ is orthogonal to the residual $\nu^1(k-1)$ and that $I^{<2,\,1>}(k|k-1)$ depends only on $\varepsilon^2(k-1)$. Notably, the orthogonal principle (15) of the proposed IMM algorithm is valuable since it can be utilized to check whether the IMM filter is consistent or not [29]. This means that the orthogonal principle (15) should be satisfied as much as possible to guarantee the consistency of the proposed IMM filter [30].

The differences between the proposed compensation algorithm and traditional STF are summarized as follows. The traditional STF is not directly applicable to the multimodel-based estimation problem because of its structure. However, the proposed compensation algorithm considers the mixing of the submodel filter when calculating the compensation parameter, as described in (14). Moreover, the negative effect of compensating $P^{0j}(k-1|k-1)$ with λ is effectively mitigated, as described in (22).

In addition, the distinctive difference between the proposed algorithm and the approaches in [29] and [30] is in how the compensation parameter λ is formulated. Equations (28) and (29) in [30] present the compensation parameter θ to modify the covariance to address the model parameter mismatch. Although the result is satisfactory to some extent, the algorithm cannot be extended into the UKF since the compensation parameter is multiplied by the weighted two-norm of the covariance. However, the proposed algorithm can easily be extended into the UKF or another approximate Bayesian filter such as the cubature Kalman filter (CKF) as shown in (24).

Moreover, the proposed compensation parameter can adaptively tune the Kalman gain matrix according to the innovation sequence. Thus, a high tracking performance can be achieved when faced with abrupt state changes caused by model mismatch. The effects of the compensation parameter have rarely been discussed in previous research, and we thoroughly analyze the effect of the compensation parameter via numerical simulation in the next section.

V. NUMERICAL SIMULATION

To assess the effectiveness of the proposed RIMM algorithm, two simulation scenarios of a maneuvering target tracking problem with artificial uncertainty are considered. To track the maneuvering target, two models are utilized by each subfilter in the IMM filter: a uniform motion model and a coordinated turn model in the horizontal plane. The proposed algorithm is compared with the conventional IMM-EKF and IMM-UKF algorithms.

A. UNIFORM MOTION MODEL

The uniform motion (UM) model with a nearly constant velocity in discrete time can be described as follows [38]:

$$x(k+1) = \begin{bmatrix} 1 & 0 & T_s & 0 \\ 0 & 1 & 0 & T_s \\ 0 & 0 & 1 & 0 \\ 0 & 0 & 0 & 1 \end{bmatrix} x(k) + \begin{bmatrix} \frac{1}{2}{T_s}^2 & 0 \\ 0 & \frac{1}{2}{T_s}^2 \\ T_s & 0 \\ 0 & T_s \end{bmatrix} w(k)_{UM} \quad (25)$$

where T_s is the sampling time interval and the state of the target (x) is defined as $x(k) = [\xi_k \ \ \eta_k \ \ \dot{\xi}_k \ \ \dot{\eta}_k]^T$. The first two states ($\xi$, η) refer to the x-axis and y-axis positions on the horizontal plane, respectively, and the last two states ($\dot{\xi}_k$, $\dot{\eta}_k$) are the velocities in the directions of the x-axis and y-axis, respectively. $w(k)_{UM}$ is the zero-mean Gaussian white noise used to represent relatively small accelerations with an appropriate covariance $Q(k)_{UM}$. It is assumed in the UM model that only x-axis and y-axis position measurements are available as follows:

$$z(k) = \begin{bmatrix} 1 & 0 & 0 & 0 \\ 0 & 1 & 0 & 0 \end{bmatrix} x(k) + \upsilon(k) \quad (26)$$

where $\upsilon(k)$ is zero-mean white Gaussian measurement noise.

B. COORDINATE TURN MODEL

The turning motion of a target usually follows a pattern termed a coordinated turn (CT), which is characterized by a nearly constant turn rate and a constant speed [22]. The CT model may be considered to be a nonlinear model if the turn rate of the target is unknown. In the CT model, the state vector needs to be augmented to include the turning rate Ω as $x = [\xi \ \ \eta \ \ \dot{\xi} \ \ \dot{\eta} \ \ \Omega]^T$. The coordinated turn model is then represented by the following [39]:

$$x(k+1) = \begin{bmatrix} 1 & 0 & \frac{\sin \Omega(k) T_s}{\Omega(k)} & \frac{\cos \Omega(k) T_s - 1}{\Omega(k)} & 0 \\ 0 & 1 & \frac{1 - \cos \Omega(k) T_s}{\Omega(k)} & \frac{\sin \Omega(k) T_s}{\Omega(k)} & 0 \\ 0 & 0 & \cos \Omega(k) T_s & -\sin \Omega(k) T_s & 0 \\ 0 & 0 & \sin \Omega(k) T_s & \cos \Omega(k) T_s & 0 \\ 0 & 0 & 0 & 0 & 1 \end{bmatrix} x(k) + \begin{bmatrix} \frac{1}{2}{T_s}^2 & 0 & 0 \\ 0 & \frac{1}{2}{T_s}^2 & 0 \\ T_s & 0 & 0 \\ 0 & T_s & 0 \\ 0 & 0 & T_s \end{bmatrix} w(k)_{CT}. \quad (27)$$

The measurement equation of the CT model is assumed to be the same as that of the UM model in that only x-axis and y-axis position measurements are available. Note that the states of the UM and CT models of the IMM algorithm differ; that is, the turning rate Ω from the state of the UM model is added to the state of the CT model, but the measurement model is the same as shown in equation (26) for the UM and CT models.

C. SIMULATION SETTING

Throughout the simulations, the units for time, position, velocity, and angular rate are s, m, m/s, and rad/s, respectively, unless otherwise stated. In the simulation, the sampling interval is set to $T_s = 0.1$ s, with 200 intervals, yielding simulation times of 20 s. The simulation scenario of the maneuvering target is the same with [40] but with modeling uncertainty and is designed as follows: The target starts from the initial position (ξ, η) = (0, 0) with a velocity ($\dot{\xi}$, $\dot{\eta}$) = (20, 0) at $t = 0$ s for 4 s. The target then begins a coordinated left turn at 4 s with a rate $\Omega = 1$ rad/s for a period of 5 s. At 9 s, the target stops turning and moves straight for 2 s with a constant velocity of 20 m/s for a period of 2 s. The target then starts a coordinated right turn with a rate $\Omega = -1$ at

11 s for a period of 5 s. Finally, the target continues to move straight for 4 s with the same velocity. To generate the ground truth simulation results, equations (25) through (27) are used to generate the true navigation trajectory and their corresponding measurements. Note that the average velocity of the maneuvering target in the simulation scenario is designed to be consistent with the experiment described in Section VI.

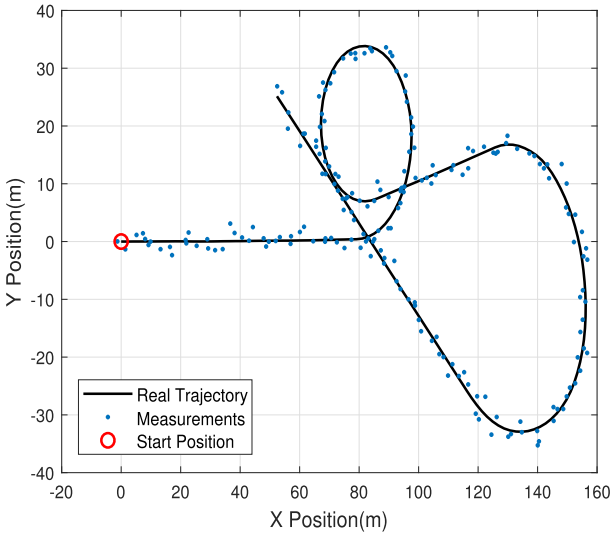

FIGURE 3. True navigation trajectory.

The resulting trajectory is plotted in Fig. 3. The variance of the process noise for the UM model is set to $Q(k)_{UM} = 0.01$, and the variance of the process noise for the CT model is set to $Q(k)_{CT} = 0.15$. The measurement noise variance for the UM and CT models is set to $R = diag([0.05\ 0.05])$. Note that the target motion is designed to be extremely slow compared to the conventional ATC scenario in this simulation to highlight the effects of the modeling uncertainty.

The initial state estimate is chosen randomly from the Gaussian distribution $N(x(0), P(0|0))$, where $x(0) = [0, 0, 1, 0, 0]^T$ is the true initial state of the maneuvering target and $P(0|0) = diag([0.1^2\ 0.1^2\ 0.1^2\ 0.1^2\ 0.1^2])$ is the corresponding covariance. The model transition probability matrix of the IMM filter is set to

$$p_{ij} = \begin{bmatrix} 0.9 & 0.1 \\ 0.1 & 0.9 \end{bmatrix}.$$

The initial model probabilities are set to $\mu(0) = \begin{bmatrix} 0.95\ 0.05 \end{bmatrix}$.

D. EVALUATION

In this simulation, 1,000 independent Monte Carlo runs of the conventional IMM-EKF/IMM-UKF algorithms and the proposed robust IMM-EKF (RIMM-EKF)/UKF (RIMM-UKF) algorithms are performed and analyzed. All filters are programmed with MATLAB 2017b on a PC with an Intel Core i7-6500U CPU at 2.50 GHz. The root mean square error (RMSE), averaged RMSE (ARMSE), and averaged absolute value of biases (AAVB) of the position metrics are utilized to evaluate the performance:

$$RMSE_{pos}(k) = \sqrt{\frac{1}{M}\sum_{m=1}^{M}((\xi_{m,k} - \hat{\xi}_{m,k})^2 + (\eta_{m,k} - \hat{\eta}_{m,k})^2)}$$

$$ARMSE_{pos} = \sqrt{\frac{1}{M}\frac{1}{T}\sum_{k=1}^{T}\sum_{m=1}^{M}((\xi_{m,k} - \hat{\xi}_{m,k})^2 + (\eta_{m,k} - \hat{\eta}_{m,k})^2)}$$

$$AAVB_{pos} = \frac{1}{T}\sum_{k=1}^{T}\left|\frac{1}{M}\sum_{m=1}^{M}(\xi_{m,k} - \hat{\xi}_{m,k})\right| + \frac{1}{T}\sum_{k=1}^{T}\left|\frac{1}{M}\sum_{m=1}^{M}(\eta_{m,k} - \hat{\eta}_{m,k})\right|$$

where T and M refer to the simulation duration and iteration number of the Monte Carlo simulation, respectively; $(\xi,\ \eta)$ is the true value of the target position; and $(\hat{\xi},\ \hat{\eta})$ is the estimated position at time k in the m-th Monte Carlo simulation. The RMSE, ARMSE, and AAVB of the velocity can be formulated in the same manner. The AAVB performance metric is often utilized to analyze the bias of state estimates. In other words, a smaller AAVB means that the state estimate is more likely to be unbiased [41].

In this simulation, to demonstrate the validity of the proposed RIMM filter under modeling uncertainty, four different test cases, such as inaccurate covariances of the process noise for the UM model (Scenario 1) and CT model (Scenario 2), are performed, as summarized in (28) and Table 3.

$$w^j(k) \sim \begin{cases} N(0, Q(k)_{model}) & \text{w.p. } 1 - p_c \\ N(0, \rho \times Q(k)_{model}) & \text{w.p. } p_c \end{cases} \tag{28}$$

where w.p. denotes "with probability", $Q(k)_{model} = Q(k)_{UM}$ or $Q(k)_{CT}$, and ρ is the multiplier factor that represents the degree of the modeling uncertainty. Equation (28) means that $w^j(k)$ is drawn from $N(0, Q(k)_{model})$ with probability $1 - p_c$ and $N(0, \rho \times Q(k)_{model})$ with probability p_c. The multiplier factor ρ depends on the simulation test scenario, as shown in Table 3. In this simulation, p_c is set to 0.7. Scenario 1 refers to a situation in which artificial modeling uncertainty is injected into the UM model, while keeping the process noise of the CT model constant, whereas Scenario 2 refers to a situation in which artificial modeling uncertainty is injected into the CT model, while keeping the process noise of the UM model constant.

The RMS position and velocity errors for 1,000 Monte Carlo runs during Scenario 1 are shown in Figs. 4(a) and 4(b), respectively. It can be observed during the time intervals of 0-4 s, 9-11 s, and 16-20 s with process noise covariance that the estimation errors of the IMM-EKF and IMM-UKF algorithms increase significantly, whereas because of the modeling uncertainty compensation algorithm, the estimation errors under the RIMM-EKF and RIMM-UKF algorithms are much smaller, leading to improved filtering accuracy. Similarly, Figs. 5(a) and 5(b) show the RMS position and velocity errors

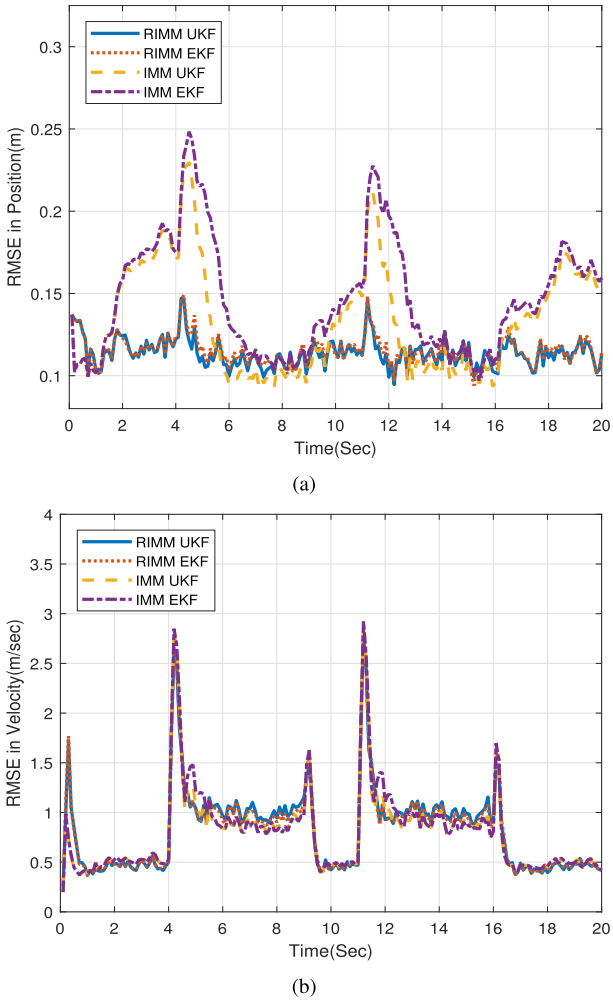

FIGURE 4. (a) RMSEs of the position estimates of the proposed method and the conventional method (Scenario 1, Case 2). (b) RMSEs of the velocity estimates of the proposed method and the conventional method (Scenario 1, Case 2).

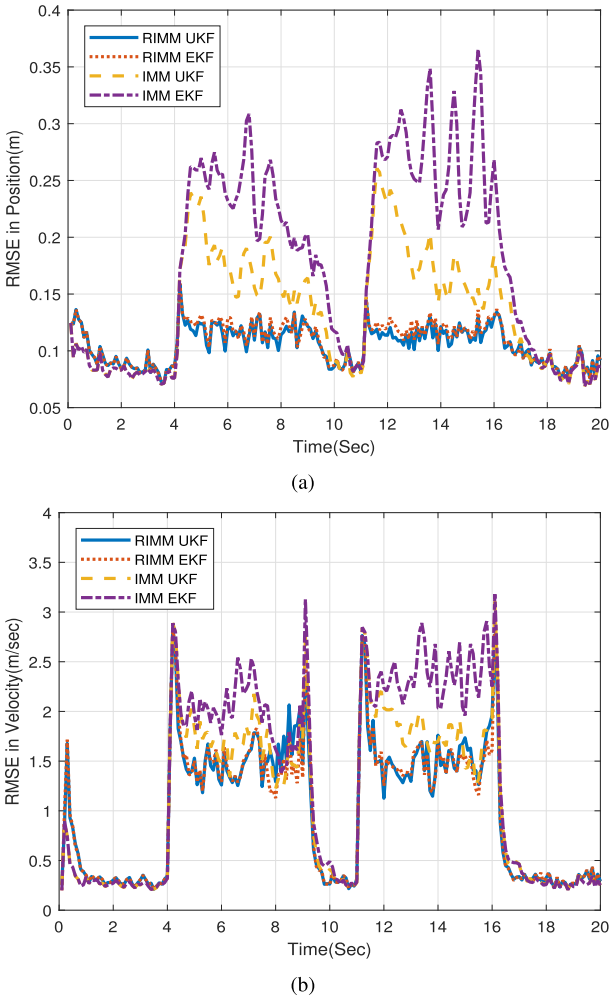

FIGURE 5. (a) RMSEs of the position estimates of the proposed method and the conventional method (Scenario 2, Case 2). (b) RMSEs of the velocity estimates of the proposed method and the conventional method (Scenario 2, Case 2).

for 1,000 Monte Carlo runs during Scenario 2. It can also be observed during the time intervals of 5-9 s and 11-16 s with process noise covariance that the estimation errors of the IMM-EKF and IMM-UKF algorithms increase significantly, whereas the estimation errors of the RIMM-EKF and RIMM-UKF algorithms are much smaller, leading to improved robustness of the filter.

The ARMSEs of the position, velocity, and course heading errors and the AAVB of the position velocity obtained by each algorithm for the four test cases are summarized in Tables 1 and 2, respectively. The ARMSEs of the position, velocity, and course heading errors obtained by the proposed RIMM-EKF and RIMM-UKF algorithms are substantially smaller than those obtained by the IMM-EKF and IMM-UKF algorithms. Furthermore, the AAVB of the position and velocity from the proposed RIMM-EKF and RIMM-UKF algorithms are smaller than those from the conventional IMM-EKF and IMM-UKF algorithms because the introduction of the modeling uncertainty compensation parameter decreases the effect of the modeling uncertainty. In addition, as expected, the UKF provides more accurate estimates than the EKF because no linearization of the coordinated turn model is required. Finally, the proposed robust algorithm has a more profound effect on the estimation performance of Case 2 than that of Case 1 because the process noise covariances of Case 2 are increased by a factor of 100.

In the compensation step, the modeling uncertainty parameter λ in the IMM filter should be automatically adjusted to effectively address the inaccuracies of the model used in the filter. Figs. 6(a) and 6(b) show the online change in the modeling uncertainty parameter λ for Scenarios 1 and 2. Note that the λ of the IMM-EKF and IMM-UKF algorithms is computed using only (21) since the modeling uncertainty compensation step is not incorporated into the IMM-EKF and IMM-UKF algorithms. It can be observed during the time intervals of 0-4 s, 9-11 s, and 16-20 s with process noise covariance that the λ values of the IMM-EKF and IMM-UKF methods increase considerably because IMM-EKF and IMM-EKF do not incorporate the modeling uncertainty compensation step. This indicates that

TABLE 1. Performance comparison for Scenario 1.

Algorithm	Position ARMSE (m)		Velocity ARMSE (m/s)		Course Heading ARMSE (rad)	
	Case 1	Case 2	Case 1	Case 2	Case 1	Case 2
RIMM-UKF	0.1039	0.1134	0.9074	0.9197	0.1277	0.1327
RIMM-EKF	0.1054	0.1155	0.8973	0.9174	0.1289	0.1333
IMM-UKF	0.1068	0.1354	0.8458	0.8898	0.1291	0.1332
IMM-EKF	0.1204	0.1497	0.8639	0.9143	0.1298	0.1345
Algorithm	Position AAVB (m)		Velocity AAVB (m/s)			
	Case 1	Case 2	Case 1	Case 2		
RIMM-UKF	0.1150	0.1263	0.7803	0.8297		
RIMM-EKF	0.1172	0.1292	0.7924	0.8595		
IMM-UKF	0.1176	0.1462	0.8140	0.8366		
IMM-EKF	0.1327	0.1642	0.8251	0.8652		

TABLE 2. Performance comparison for Scenario 2.

Algorithm	Position ARMSE (m)		Velocity ARMSE (m/s)		Course Heading ARMSE (rad)	
	Case 1	Case 2	Case 1	Case 2	Case 1	Case 2
RIMM-UKF	0.1052	0.1067	0.9740	1.1143	0.1187	0.1295
RIMM-EKF	0.1078	0.1089	0.9846	1.2005	0.1287	0.1305
IMM-UKF	0.1139	0.1451	0.9836	1.3633	0.1327	0.1312
IMM-EKF	0.1348	0.1940	1.0330	1.6407	0.1432	0.1345
Algorithm	Position AAVB (m)		Velocity AAVB (m/s)			
	Case 1	Case 2	Case 1	Case 2		
RIMM-UKF	0.1157	0.1175	0.8772	1.0180		
RIMM-EKF	0.1189	0.1203	0.8819	1.0265		
IMM-UKF	0.1229	0.1453	0.8975	1.1210		
IMM-EKF	0.1457	0.1845	0.9028	1.2908		

TABLE 3. Simulation test scenario.

	Scenario 1	Scenario 2
Case 1	$\rho = 10,\ w^j(k)$ for $j = UM$	$\rho = 10,\ w^j(k)$ for $j = CT$
Case 2	$\rho = 100,\ w^j(k)$ for $j = UM$	$\rho = 100,\ w^j(k)$ for $j = CT$

the orthogonality (13) condition is not guaranteed because of the incorrect process noise (i.e., increased by a factor of 10 or 100) during the time intervals of 0-4 s, 9-11 s, and 16-20 s. On the other hand, the λ values of the RIMM-EKF and RIMM-UKF algorithms remain close to 1 even during the time intervals of 0-4 s, 9-11 s, and 16-20 s because the proposed algorithm determines the compensation parameter adaptively to ensure that the innovation sequences remain orthogonal to the state estimation errors, which makes (13) true and λ remain close to 1.

Figs. 7(a) and 7(b) describe the mode probability calculated in the proposed IMM filter for Scenario 1. It can be observed that compared to the true mode probability, the mode probabilities of the proposed RIMM-EKF and RIMM-UKF algorithms are lower than those of the conventional IMM-EKF and IMM-UKF algorithms. The cause of this phenomenon may be the increase in the process noise covariance during Scenarios 1 and 2. Thus, it can be concluded that the mode probability of the proposed RIMM-EKF and RIMM-UKF algorithms better describes the true trajectory of Scenario 2 than the conventional IMM-UKF and IMM-EKF algorithms. The aforementioned results can also be found in Fig. 8(a) and 8(b) for Scenario 2.

To conduct filter consistency testing, statistical hypothesis tests were implemented [22]. An acceptance region for the filter consistency testing is defined based on the fact that under the hypothesis that the filter model is correct, the normalized innovation squared (NIS) statistic follows a chi-square distribution. Specifically, when the filter is consistent, the average NIS from N independent samples is [22]:

$$\bar{\varepsilon}_v(k) = \frac{1}{N}\sum_{k=1}^{N} \nu(k)^T S(k)\, \nu(k)$$

where $\nu^j(k)$ is the innovation sequence in the j-th subfilter of the IMM filter. The NIS is expected to follow a χ^2_n distribution, where n is the number of measurements (degrees of freedom). If $\bar{\varepsilon}_v(k)$ is outside the bounds of the chi-square

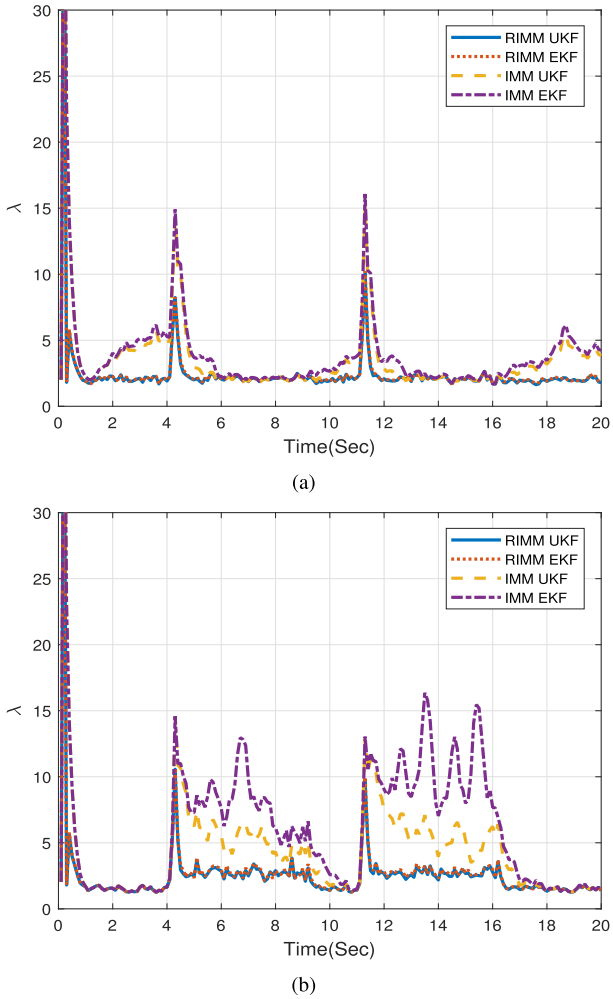

FIGURE 6. Model uncertainty compensation parameter λ (a) for Scenario 1, Case 2. (b) for Scenario 2, Case 2.

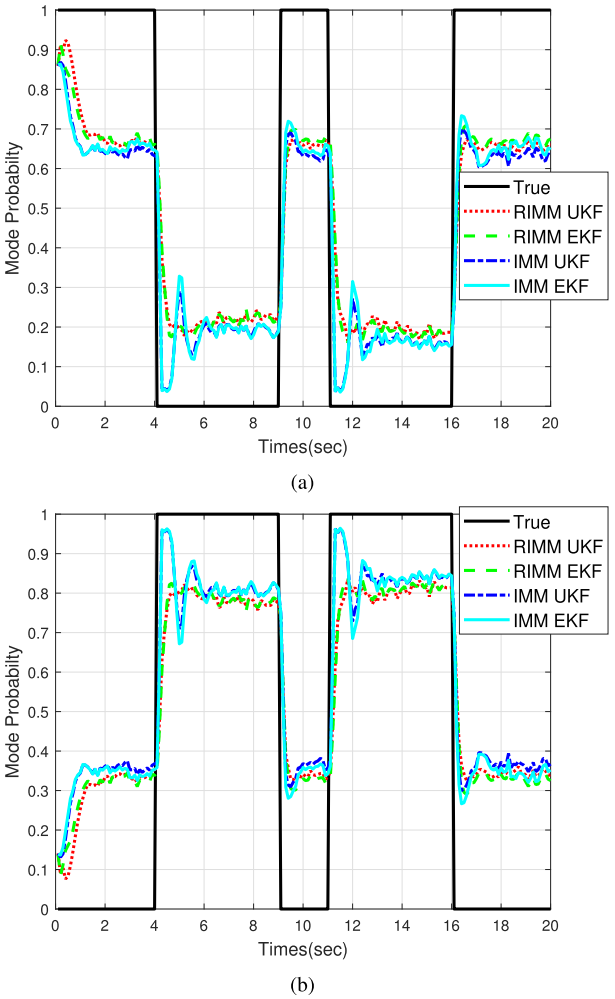

FIGURE 7. (a) Mode probability model UM (Scenario 1). (b) Mode probability model CT (Scenario 1).

distribution for a desired confidence level, implying that the innovation is abnormally large, it is concluded that there are modeling errors in the filter design.

To further analyze the credibility of the proposed algorithm, an analysis of the averaged normalized estimation error squared (ANEES) was conducted as follows [22]:

$$\bar{\varepsilon}_i(k) = \frac{1}{nM}\sum_{i=1}^{M}\varepsilon_i \tag{29}$$

where the NEES in the i-th run is defined by $\varepsilon_i = (x_i - \hat{x}_i)^T P_i^{-1}(x_i - \hat{x}_i)$. The ANEES is often used as a measure of an estimator's credibility: The closer to 1 the ANEES is, the more credible the estimator [42]. As shown in Fig. 10, the ANEES of the RIMM-EKF and RIMM-UKF is closer to 1 than that of the IMM-EKF and IMM-UKF, although a temporary increase in the ANEES can be observed.

Figs. 9(a) and 9(b) show the NIS during Scenario 1, including the upper and lower limits of χ_n^2. In this simulation, the two-sided 95% region for an $n = 2$ degrees of freedom chi-square random variable is theoretically $\left[\chi_2^2(0.025), \chi_2^2(0.975)\right] = [0.0506, \ 7.3778]$. Because the lower limit is essentially zero, only the upper limit is of interest, and it was taken for the 5% tail rather than for the 2.5% tail, which is 7.3778. It should be noted that taking a 5% or a 2.5% tail is rather arbitrary, and the design decision is based on the confidence level.

It can be observed during the time intervals of 0-4 s, 9-11 s, and 16-20 s with the process noise covariance that the NISs of the IMM-EKF and IMM-UKF are outside the bounds of the chi-square distribution for the desired confidence level (95%), whereas the NISs of the RIMM-EKF and RIMM-UKF are inside the bounds. By modifying the prior covariance by the model compensation parameter λ in the j-th subfilter of the IMM filter, the information of the system model is more lightly weighted, and hence, the information of the measurement is more heavily weighted. As a result, the undesirable impacts of the model errors are effectively minimized, thus improving the consistency of the filter and maintaining the NIS inside the bounds of the chi-square distribution, although the computational complexity of the RIMM-UKF and RIMM-EKF is slightly higher than that of the RIMM-UKF and IMM-EKF as shown in Table 4.

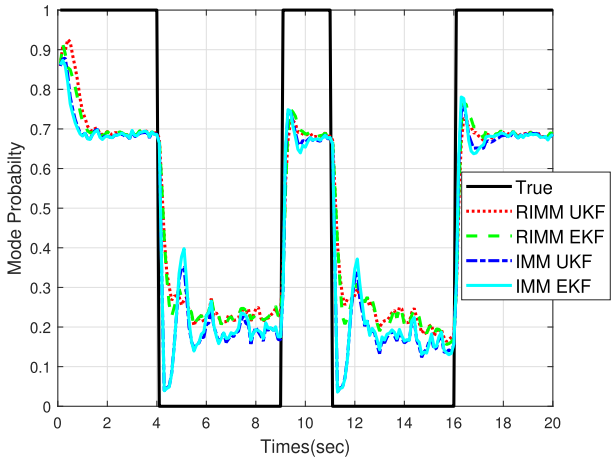

(a)

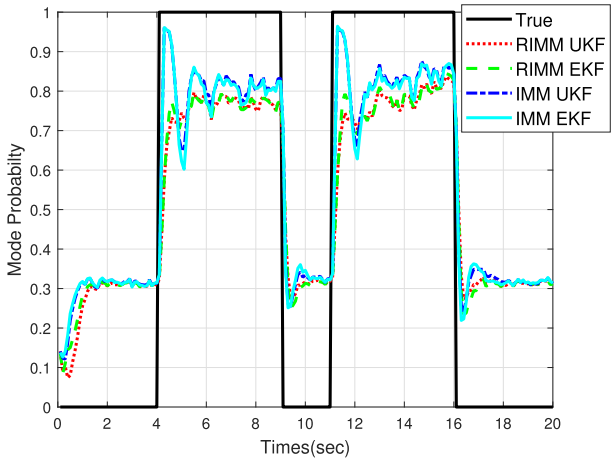

(b)

FIGURE 8. (a) Mode probability model UM (Scenario 2). (b) Mode probability model CT (Scenario 2).

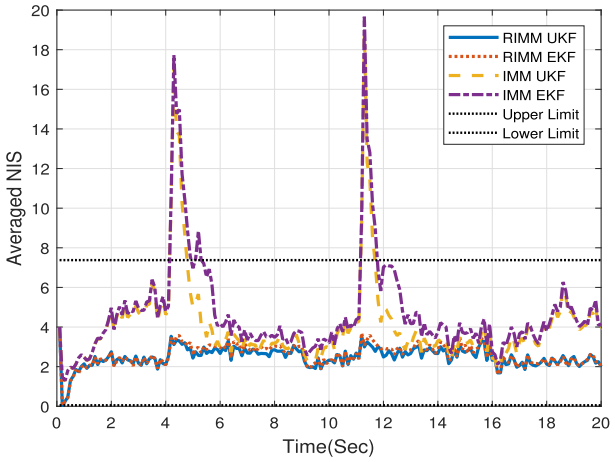

(a)

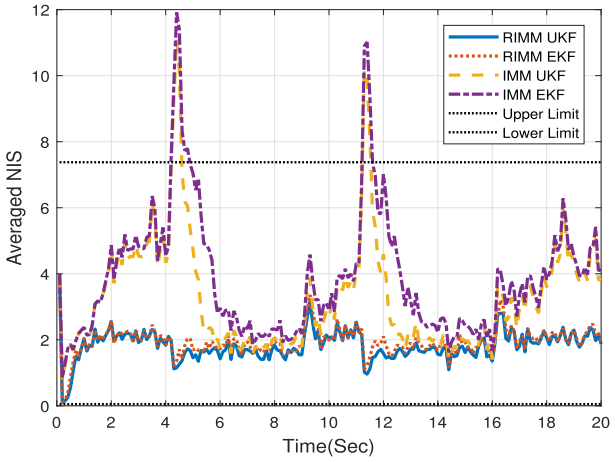

(b)

FIGURE 9. Averaged normalized innovation squared (a) Model UM (Scenario 1, Case 2). (b) Model CT (Scenario 1, Case 2). The dashed lines are the two-sided 95% χ^2_n acceptance bounds.

VI. EXPERIMENTAL RESULTS

To further evaluate the effectiveness of the proposed RIMM algorithm, car-mounted experiments using the TDOA measurements were conducted in an airport as follows.

A. EXPERIMENTAL SETUP

The fundamental principle of multilateration (MLAT) is the use of a hyperbolic curve and determination of a hyperbolic position by utilizing the TDOA of the received signal from at least four RUs, as shown in Fig. 11. One of the RUs is used as a reference, and the remaining RUs are employed to calculate the position of the MU. Among several wireless network approaches in the MLAT system, TDOA was chosen to achieve a high-accuracy measurement and to decrease the complexity of the system since accurate time synchronization is not required.

The MLAT system consists of a number of RUs, which are installed in locations known a priori around an airport. The MLAT system uses 1090 MHz Mode A/C and Mode S transponder signals to receive the squitters and replies from the aircraft. The processed TDOA measurement along

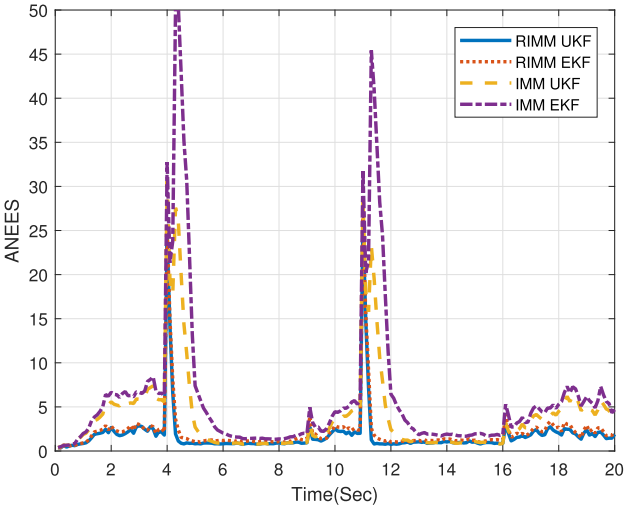

FIGURE 10. The averaged normalized estimation error squared (Scenario 1, Case 2).

with the timestamp information are collected in the central processing subsystem (CPS), where the transponder position of the MU is estimated. Since the robust filtering algorithm

TABLE 4. Computation time for Scenario 2.

	RIMM-UKF	RIMM-EKF	IMM-UKF	IMM-UKF
Time (sec)	0.1761	0.1279	0.1630	0.1176

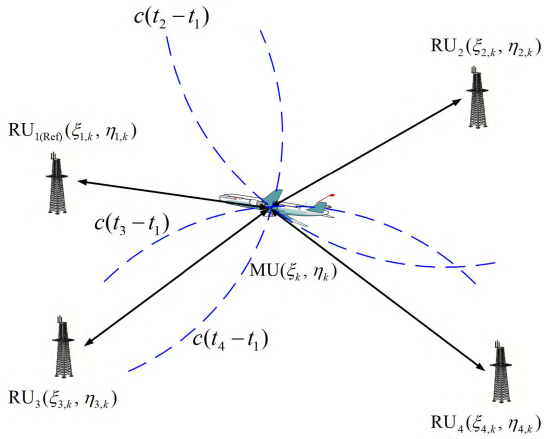

FIGURE 11. TDOA hyperbolic positioning principle in the MLAT system.

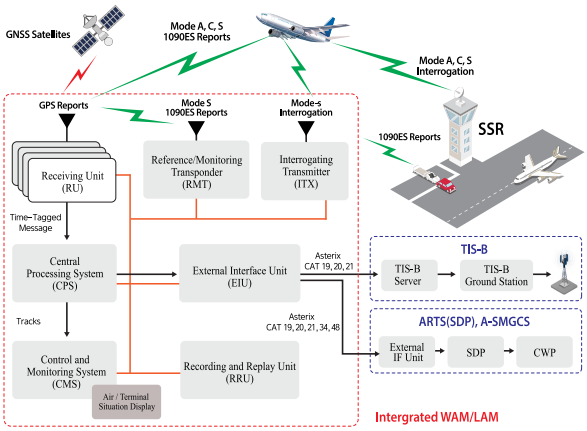

FIGURE 12. Architecture diagram of the MLAT system.

implemented in the CPS is our main focus, the detailed explanation of MLAT systems is beyond the scope of this paper and thus only briefly depicted in Fig. 12.

The TDOA measurements $z^j(k)$ ($j = 2, \cdots, m$, where m is the number of receivers) between RU_j and RU_1 in the MLAT system, as the measurement model of the UM and CT models, can be expressed as follows:

$$\begin{aligned} z^j(k) &= \sqrt{(\xi_k - \xi_{j,k})^2 + (\eta_k - \eta_{j,k})^2} \\ &\quad - \sqrt{(\xi_k - \xi_{1,k})^2 + (\eta_k - \eta_{1,k})^2} \\ &= c(t_i - t_1) + v^j(k) \end{aligned} \tag{30}$$

$$z(k) = \begin{bmatrix} z^2(k) \\ \vdots \\ z^m(k) \end{bmatrix} = \begin{bmatrix} c(t_2 - t_1) \\ \vdots \\ c(t_m - t_1) \end{bmatrix} + \begin{bmatrix} v^2(k) \\ \vdots \\ v^m(k) \end{bmatrix} \tag{31}$$

where ξ_k and η_k refer to the x and y positions of the MU at time index k. $\xi_{j,k}$ and $\eta_{j,k}$ refer to the x and y positions of RU_j, and RU_1 refers to the reference RU. $v^j(k)$ is zero-mean white

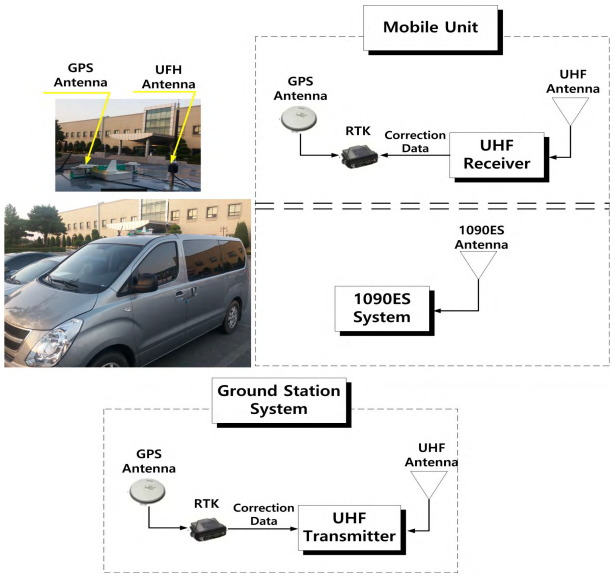

FIGURE 13. Setup of car-mounted experiment.

FIGURE 14. Navigation trajectory and the location of the installed RUs with antennas.

Gaussian measurement noise of RU_j. $c = 3 \times 10^8$ ms^{-1} is the approximate speed of light.

To verify the proposed RIMM algorithm, car-mounted experiments were conducted. A single-antenna GPS receiver, a mode S transponder, and a UHF antenna were utilized in these experiments, as depicted in Fig. 13. The field experiment was conducted at Hanseo University, Korea. Fig. 14 depicts the test site and the navigation trajectory. Ten RUs were installed as shown in Fig. 14. The data from an RTK-GPS (Novatel) at 20 Hz were recorded and considered to be the ground-truth data. TDOA measurements were collected for a period of approximately 850 s. The average velocity of the car is approximately 20 m/sec during the experiments. The sampling interval T_s for the position update was 1 s. Note that the process noise matrix $\mathbf{Q}$ is empirically selected by trial and error, while the measurement noise matrix $\mathbf{R}$ is determined from the static test for the RU.

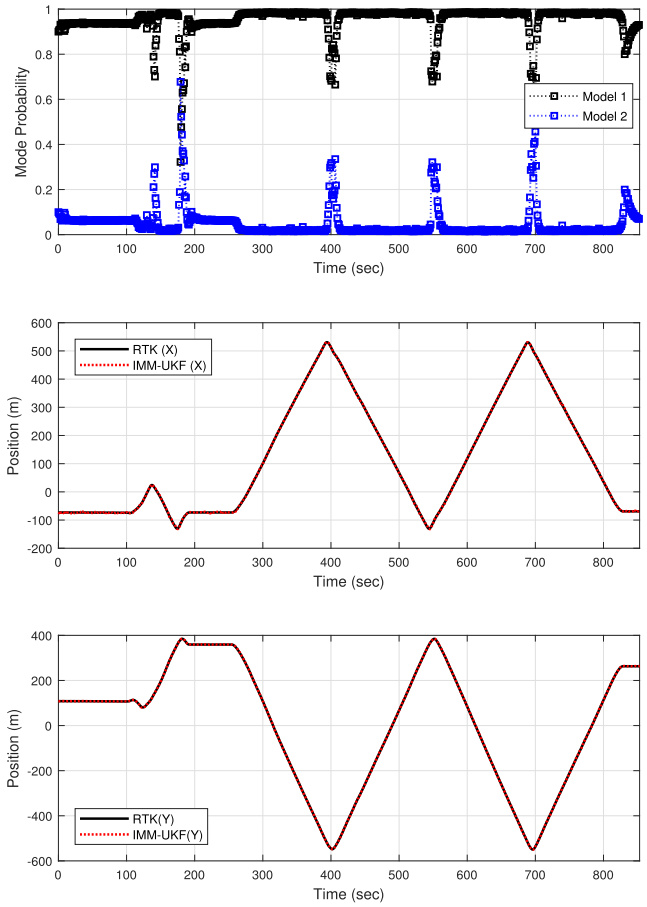

FIGURE 15. Mode probability of the IMM-UKF with the UM and CT models and the corresponding estimated x and y positions (no modeling uncertainty case).

First, the no modeling uncertainty case was considered. As shown in Fig. 14, the navigation trajectory can be approximated as the combination of the UM and CT models. Thus, the UM and CT model is utilized as the subfilter and $\mathbf{Q}$ is set to $diag([10\ ,\ 10\ ,\ 5\ ,\ 5])$ and $diag([10\ ,\ 10\ ,\ 5\ ,\ 5\ ,\ 1])$ for the UM and CT models, respectively, and $\mathbf{R}$ is set to $4.5\mathrm{I}_{m\times m}$. The initial mode probabilities of the IMM filter were set to $\mu(0) = \begin{bmatrix}0.85 & 0.15\end{bmatrix}$. The model transition probability matrix of the IMM filter was set to

$$p_{ij} = \begin{bmatrix}0.8 & 0.2\\ 0.2 & 0.8\end{bmatrix}.$$

Fig. 15 shows the mode probabilities of the UM model (model 1) and CT model (model 2) and the corresponding x and y positions. As shown, the mode probability of the conventional IMM-UKF algorithm correctly describes the true trajectory, that is, the mode probability of the CT model (model 2) rapidly increases during the turning motion of the vehicle. In addition, the position estimate of the IMM-UKF with the UM and CT models closely follows the true RTK data. Thus, the IMM-UKF with the UM and CT models (IMM-UKF (UM, CT)) is considered the true model without the modeling uncertainty.

B. EVALUATION

To assess the proposed RIMM-UKF algorithm under modeling uncertainty, two CT models corresponding to different turn rates are used, that is, -1 rad/s and 0 rad/s. As the turn rate Ω of the CT model approaches zero, it can be regarded as an approximation of the UM model [43]. However, two CT models corresponding to different turn rates do not exactly match the true navigation trajectory, as shown in Fig. 14. In other words, the models used in the proposed RIMM-UKF algorithm do not describe the true navigation trajectory, and thus, modeling uncertainty or mismatch against the true model exists. In the RIMM-UKF with two CT models (RIMM-UKF (CT, CT)), the initial mode probabilities were set to $\mu(0) = \begin{bmatrix}0.85 & 0.15\end{bmatrix}$. The model transition probability matrix of the RIMM-UKF (CT, CT) was set to

$$p_{ij} = \begin{bmatrix}0.85 & 0.15\\ 0.15 & 0.85\end{bmatrix}.$$

The logarithmic localization errors (LLEs), root mean square errors (RMSEs), AAVBs, and max absolute errors (MAEs) of the position metrics were considered to evaluate the performance. The LLE, RMSE, and AAVB are, respectively, defined as follows:

$$LLE(k) = log_{10}\left\{\sqrt{(\xi_k - \hat{\xi}_k)^2 + (\eta_k - \hat{\eta}_k)^2}\right\} \quad (32)$$

$$RMSE = \sqrt{\frac{1}{T}\sum_{k=1}^{T}(\xi_k - \hat{\xi}_k)^2 + (\eta_k - \hat{\eta}_k)^2} \quad (33)$$

$$AAVB = \frac{1}{T}\sum_{k=1}^{T}\left|\xi_k - \hat{\xi}_k\right| + \left|\eta_k - \hat{\eta}_k\right|. \quad (34)$$

TABLE 5. Performance comparison of the position RMSE, AAVB, and MAE for different algorithms.

Algorithm	Position RMSE (m)	Position AAVB (m)	Position MAE (m)
IMM-UKF (UM, CT)	1.78	1.77	6.12
IMM-UKF (CT, CT)	4.26	2.55	58.10
RIMM-UKF (CT, CT)	2.12	2.17	8.81

Table. 5 summarizes the estimation performance results. Note that only the UKF filter is utilized as the individual subfilter in the experiment since the UKF provides more accurate estimates than the EKF. Although the estimation performance of the RIMM-UKF (CT, CT) is slightly lower than that of the IMM-UKF (UM, CT), the proposed RIMM-UKF (CT, CT) outperforms the IMM-UKF (CT, CT) in terms of the position RMSE, AAVB and MAE. Fig. 16 also depicts the LLEs of the three approaches. It can be seen that the position estimate of the IMM-UKF (CT, CT) often significantly deviates from the true trajectory, while the position estimate of the RIMM-UKF (CT, CT) closely follows the true trajectory. This deviation of the IMM-UKF (CT, CT) is attributable to the absence of the modeling uncertainty compensation. It can be concluded that the proposed RIMM-UKF (CT, CT) algorithm exhibits robustness against modeling uncertainty.

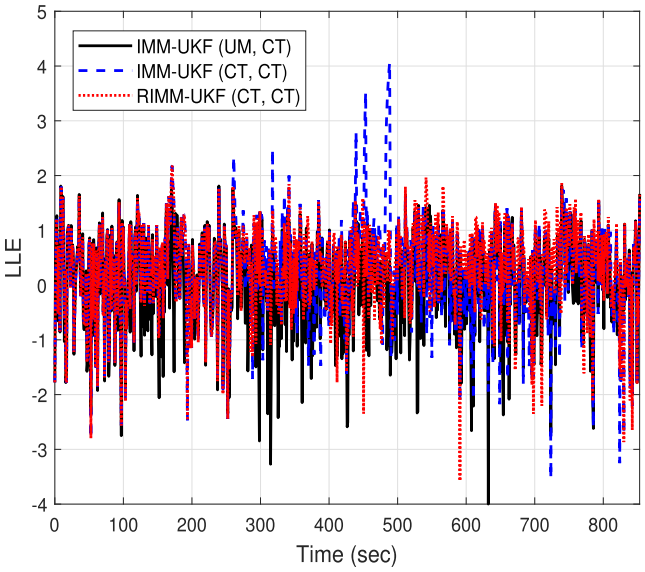

FIGURE 16. LLE of IMM-UKF (UM, CT), IMM-UKF (CT, CT), and RIMM-UKF (CT, CT).

VII. CONCLUSION

In this paper, a robust IMM is proposed for target tracking modeled by a combination of multiple linear/nonlinear stochastic hybrid systems with uncertain model parameters. An uncertainty compensation procedure is devised to change the prior variances to satisfy the proposed orthogonality condition as much as possible, thus improving the consistency of the filter. To verify the effectiveness of the proposed algorithm, numerical simulations and a car-mounted experiment in an airport using the TDOA measurement are conducted. The experimental results show that compared with the conventional IMM-EKF and IMM-UKF methods, the proposed RIMM-EKF and RIMM-UKF methods achieve better target tracking estimation accuracies with smaller biases. This result is attributable to the incorporation of the modeling uncertainty compensation algorithm, which effectively changes the covariance in the proposed robust filters, thus alleviating the undesirable influence of the inaccurate model on the state estimation solution. Therefore, it can be concluded that the proposed RIMM algorithm has strong robustness to model parameter mismatch for maneuvering target tracking with changing dynamics.

REFERENCES

[1] H. Zhang, J. Xie, J. Ge, W. Lu, and B. Zong, "Adaptive strong tracking square-root cubature Kalman filter for maneuvering aircraft tracking," *IEEE Access*, vol. 6, pp. 10052–10061, 2018.

[2] K. Punithakumar, T. Kirubarajan, and A. Sinha, "Multiple-model probability hypothesis density filter for tracking maneuvering targets," *IEEE Trans. Aerosp. Electron. Syst.*, vol. 44, no. 1, pp. 87–98, Jan. 2008.

[3] J. Kichun, C. Keounyup, and S. Myoungho, "Interacting multiple model filter-based sensor fusion of GPS with in-vehicle sensors for real-time vehicle positioning," *IEEE Trans. Intell. Transp. Syst.*, vol. 13, no. 1, pp. 329–343, Mar. 2012.

[4] S. Lee and I. Hwang, "Interacting multiple model estimation for spacecraft maneuver detection and characterization," in *Proc. AIAA Guid., Navigat., Control Conf. (AIAA)*, 2015, pp. 1333–1342.

[5] Y. Bar-Shalom, K. C. Chang, and H. A. P. Blom, "Tracking a maneuvering target using input estimation versus the interacting multiple model algorithm," *IEEE Trans. Aerosp. Electron. Syst.*, vol. 25, no. 2, pp. 296–300, Mar. 1989.

[6] H. A. P. Blom and Y. Bar-Shalom, "The interacting multiple model algorithm for systems with Markovian switching coefficients," *IEEE Trans. Autom. Control*, vol. 33, no. 8, pp. 780–783, Aug. 1988.

[7] J. E. Gray and W. Murray, "A derivation of an analytic expression for the tracking index for the alpha-beta-gamma filter," *IEEE Trans. Aerosp. Electron. Syst.*, vol. 29, no. 3, pp. 1064–1065, Jul. 1993.

[8] S. P. Ebenezer and A. Papandreou-Suppappola, "Multiple transition mode multiple target track-before-detect with partitioned sampling," in *Proc. IEEE Conf. Acoust., Speech Signal Process. (ICASSP)*, May 2014, pp. 8008–8012.

[9] H. Sheng, W. Zhao, and J. Wang, "Interacting multiple model tracking algorithm fusing input estimation and best linear unbiased estimation filter," *IET Radar Sonar Navigat.*, vol. 11, no. 1, pp. 70–77, 2016.

[10] Y. Yang and W. Gao, "An optimal adaptive Kalman filter," *J. Geodesy*, vol. 80, no. 4, pp. 177–183, 2006.

[11] G. Chang, "Robust Kalman filtering based on Mahalanobis distance as outlier judging criterion," *J. Geodesy*, vol. 88, no. 4, pp. 391–401, Jan. 2014.

[12] M. Karasalo and X. Hu, "An optimization approach to adaptive Kalman filtering," *Automatica*, vol. 47, no. 8, pp. 1785–1793, 2011.

[13] Q. Wu, Q. Jia, J. Shan, and X. Meng, "Angular velocity estimation based on adaptive simplified spherical simplex unscented Kalman filter in GFSINS," *J. Aerosp. Eng.*, vol. 228, no. 8, pp. 1375–1388, 2014.

[14] X. Wang, X. Shao, D. Gong, and D. Duan, "Improved adaptive Huber filter for relative navigation using global position system," *Proc. Inst. Mech. Eng. G, J. Aerosp. Eng.*, vol. 225, no. 7, pp. 769–777, 2011.

[15] X. Gao, D. You, and S. Katayama, "Seam tracking monitoring based on adaptive Kalman filter embedded Elman neural network during high-power fiber laser welding," *IEEE Trans. Ind. Electron.*, vol. 59, no. 11, pp. 4315–4325, Nov. 2012.

[16] G. Agamennoni, J. I. Nieto, and E. M. Nebot, "Approximate inference in state-space models with heavy-tailed noise," *IEEE Trans. Signal Process.*, vol. 60, no. 10, pp. 5024–5037, Oct. 2012.

[17] Y. Huang, Y. Zhang, N. Li, S. M. Naqvi, and J. Chambers, "A robust Student's t based cubature filter," in *Proc. 19th Int. Conf. Inf. Fusion*, Jul. 2016, pp. 9–16.

[18] Y. Huang, Y. Zhang, N. Li, Z. Wu, and J. A. Chambers, "A novel robust Student's t-based Kalman filter," *IEEE Trans. Aerosp. Electron. Syst.*, vol. 53, no. 3, pp. 1545–1554, Jun. 2017.

[19] Y. Huang, Y. Zhang, N. Li, and J. Chambers, "A robust Gaussian approximate fixed-interval smoother for nonlinear systems with heavy-tailed process and measurement noises," *IEEE Signal Process. Lett.*, vol. 23, no. 4, pp. 468–472, Apr. 2016.

[20] XR. Li, X. Zwi, and Y. Zwang, "Multiple-model estimation with variable structure. III. Model-group switching algorithm," *IEEE Trans. Aerosp. Electron. Syst.*, vol. 35, no. 1, pp. 225–241, Jan. 1999.

[21] X. R. Li, "Multiple-model estimation with variable structure. II. Model-set adaptation," *IEEE Trans. Autom. Control*, vol. 45, no. 11, pp. 2047–2060, Nov. 2000.

[22] Y. Bar-Shalom, X. R. Li, and T. Kirubarajan, *Estimation With Applications to Tracking and Navigation: Theory, Algorithms and Software*. New York, NY, USA: Wiley, 2004.

[23] M. S. Grewal and A. P. Andrews, *Kalman Filtering: Theory and Practice With MATLAB*. New York, NY, USA: Wiley, 2014.

[24] E. A. Wan and R. Van Der Merwe, "The unscented Kalman filter for nonlinear estimation," in *Proc. IEEE Conf. Adapt. Syst. Signal Process., Commun., Control Symp. (AS-SPCC)*, Oct. 2000, pp. 153–158.

[25] J. L. Crassidis and F. L. Markley, "Unscented filtering for spacecraft attitude estimation," *J. Guid., Control, Dyn.*, vol. 26, no. 4, pp. 536–542, Jul. 2003.

[26] L. Ljung, "Asymptotic behavior of the extended Kalman filter as a parameter estimator for linear systems," *IEEE Trans. Autom. Control*, vol. 24, no. 1, pp. 36–50, Feb. 1979.

[27] M. Rhudy and Y. Gu, "Understanding nonlinear Kalman filters part 1: Selection of EKF or UKF," *Interact. Robot. Lett.*, vol. 1, no. 1, pp. 1–9, 2013.

[28] D. H. Zhou and P. M. Frank, "Strong tracking filtering of nonlinear time-varying stochastic systems with coloured noise: Application to parameter estimation and empirical robustness analysis," *Int. J. Control*, vol. 65, no. 2, pp. 295–307, Oct. 1996.

[29] S. Zhao, B. Huang, X. Luan, Y. Yin, and F. Liu, "Robust fault detection and diagnosis for multiple-model systems with uncertainties," *IFAC-PapersOnLine*, vol. 48, no. 21, pp. 137–142, 2015.
[30] S. Zhao, B. Huang, and F. Liu, "Detection and diagnosis of multiple faults with uncertain modeling parameters," *IEEE Trans. Control Syst. Technol.*, vol. 25, no. 5, pp. 1873–1881, Sep. 2017.
[31] P. Maybeck, *Stochastic Models, Estimation, and Control*, vol. 3. New York, NY, USA: Academic, 1982.
[32] Q. Liu, C. Huang, and L. Peng, "Distributed consensus strong tracking filter for wireless sensor networks with model mismatches," *Int. J. Distrib. Sens. Netw.*, vol. 13, no. 11, pp. 76–86, 2017.
[33] D. Simon, *Optimal State Estimation: Kalman, H_∞, and Nonlinear Approaches*. Hoboken, NJ, USA: Wiley, 2006.
[34] D. Zhou, Y. G. Xi, and Z. Zhang, "A suboptimal multiple fading extended Kalman filter," *Chin. J. Autom.*, vol. 4, no. 2, pp. 145–152, 1992.
[35] X.-X. Wang, L. Zhao, Q.-X. Xia, and Y. Hao, "Strong tracking filter based on unscented transformation," *Control Decis.*, vol. 25, no. 10, pp. 1063–1068, Jul. 2010.
[36] P. D. Groves, *Principles of GNSS, Inertial, and Multisensor Integrated Navigation Systems*. Norwood, MA, USA: Artech House, 2013.
[37] J. A. Farrell, *Aided Navigation: GPS With High Rate Sensors*. New York, NY, USA: McGraw-Hill, 2008.
[38] E. Mazor, A. Averbuch, Y. Bar-Shalom, and J. Dayan, "Interacting multiple model methods in target tracking: A survey," *IEEE Trans. Aerosp. Electron. Syst.*, vol. 34, no. 1, pp. 103–123, Jan. 1998.
[39] X. Lin, T. Kirubarajan, Y. Bar-Shalom, and S. Maskell, "Comparison of EKF, pseudo-measurement, and particle filters for a bearing-only target tracking problem," in *Proc. SPIE, Conf. Signal Data Process. Small Targets*, 2002, pp. 240–250.
[40] S. Särkkä, J. Hartikainen, and A. Solin, "EKF/UKF toolbox for MATLAB v1.3," Centre Excellence Comput. Complex Syst. Res., Helsinki Univ. Technol., Espoo, Finland, 2007.
[41] Y. Huang, Y. Zhang, P. Shi, Z. Wu, J. Qian, and J. A. Chambers, "Robust Kalman filters based on Gaussian scale mixture distributions with application to target tracking," *IEEE Trans. Syst., Man, Cybern., Syst.*, to be published.
[42] M. Longbin, S. Xiaoquan, Z. Yiyu, S. Z. Kang, and Y. Bar-Shalom, "Unbiased converted measurements for tracking," *IEEE Trans. Aerosp. Electron. Syst.*, vol. 34, no. 3, pp. 1023–1027, Jul. 1998.
[43] H.-S. Kim, J. G. Park, and D. Lee, "Adaptive fuzzy IMM algorithm for uncertain target tracking," *Int. J. Control Autom. Syst.*, vol. 7, no. 6, pp. 1001–1008, Jun. 2009.

WONKEUN YOUN received the B.S. degree from Handong Global University, Pohang, South Korea, in 2008, and the M.S. degree from the Korea Advanced Institute of Science and Technology (KAIST), Daejeon, South Korea, in 2010, where he is currently pursuing the Ph.D. degree with the Department of Robotics Program.

He has been a Senior Researcher with the Korea Aerospace Research Institute (KARI), since 2011. His current research interests include variational Bayesian inference, Bayesian filters, multimodel target tracking, GPS/INS-based UAV navigation, and GPS-denied UAV navigation.

HYUN MYUNG received the B.S., M.S., and Ph.D. degrees from the Korea Advanced Institute of Science and Technology (KAIST), Daejeon, South Korea, in 1992, 1994, and 1998, respectively, all in electrical engineering.

He was a Senior Researcher with the Electronics and Telecommunications Research Institute, Daejeon, from 1998 to 2002. He was a CTO and the Director of the Digital Contents Research Laboratory, Emersys Corporation, Daejeon, from 2002 to 2003. He was a Principal Researcher with the Samsung Advanced Institute of Technology, Yongin, South Korea, from 2003 to 2008. Since 2008, he has been a Professor with the Department of Civil and Environmental Engineering, KAIST, where he is currently the Head of the Robotics Program. Since 2019, he has been a Professor with the School of Electrical Engineering. His current research interests include structural health monitoring using robotics, artificial intelligence, simultaneous localization and mapping, robot navigation, machine learning, deep learning, and swarm robots.